Electronic supplementary information

Nitrogen-doped porous carbon material derived from metal–organic gel for small biomolecular sensing

*Yung-Han Shih, Jian-Hong Chen, Yaling Lin, Hsin-Tsung Chen, Chia-Her Lin and Hsi-Ya Huang**

Dr. Yung-Han Shih, Jian-Hong Chen, Yaling Lin, Dr. Hsin-Tsung Chen, Prof. Chia-Her Lin, Prof. Hsi-Ya Huang
Department of Chemistry, Chung Yuan Christian University, 200 Chung Pei Road, Chung Li District, Taoyuan City, Taiwan, 320, R.O.C.
E-mail: H.-Y. Huang hyhuang@cycu.edu.tw

1. Preparation of MOGs

Cr-MOG, [Cr(OH)(BDC)], was hydrothermally synthesized under hydrothermal reactions. A mixture of chromium nitrate nonahydrate ($Cr(NO_3)_3 \cdot 9H_2O$, 0.080 g, 0.2 mmol), 1,4-benzenedicarboxylic acid (C_6H_4-1,4-$(CO_2H)_2$, BDC, 0.0786 g, 0.3 mmol) and dimethylformamide (DMF)(10 mL) was mixed in a 23 mL Teflon autoclave. The mixture was heated from 30 ℃ to 120 ^{o}C at rate of 60 ℃ h^{-1}, then kept at 120 ℃ for 8 h. After cooling to room temperature, the green wet gel was formed (Fig. S1). The MOG was activated by drying at 120 ^{o}C for 2 days then washed with ethanol (EtOH) for 5 times before further experiments.

Cr-MOG-NH_2, [Cr(OH)(BDC-NH_2]. The reaction mixture of chromium nitrate nonahydrate ($Cr(NO_3)_3 \cdot 9H_2O$, 0.080 g, 0.2 mmol), 2-amino-1,4-benzenedicarboxylic acid (BDC-NH_2, 0.0788 g, 0.3 mmol), and DMF (10.0 mL) was prepared in Teflon autoclave, then heated from 30 ℃ to 120 ^{o}C at rate of 60 ℃ h^{-1}, then kept at 120 ℃ for 8 h. After cooling to room temperature, the dark-yellow wet gel was formed (Fig. S1). The MOG was activated by drying at 120 ^{o}C for 2 days then washed with EtOH for 5 times before further experiments.

2. Characteristics of MOGs

Unlike most MOF materials with single particles, the scanning electron microscopy (SEM) and transmission electron microscopy (TEM) images indicated that the morphology of MOGs were irregular with layer-by-layer stacking (Fig. S2). Powder X-ray diffraction (PXRD) patterns of the MOGs were broad and weak but still similar with MIL-101(Cr) (Fig. S3), showing that most of the as-synthesized MOGs belong to amorphous microstructures and some of the crystalline components of MOF structure, built up by the stacking of $Cr_3(OH)(H_2O)_2O(BDC)_3$, also contained in the gels.

3. Synthesis and characterization of carbonized MOGs

MOGs powders of 0.2 g were placed into a ceramic boat then transferred in the tube furnace. The furnace was then heated under $N_{2(g)}$ flow from room temperature to 500, 600, 700, 800, and 900 ^{o}C at heating rate of 5 ^{o}C min^{-1} (refereed as cMOG-N-500-900). After the temperature reached the established settings, it was maintained for 5 h and then cooled to room temperature at rate of 1 ^{o}C min^{-1}. Except particular mentioned in the text, the cMOG-N-900 or cMOG-900 was abbreviated to cMOG-N and cMOG, respectively. Before the characterization analysis, the cMOGs were dried under vacuum at 120^{o}C overnight. The high resolution transmission electron microscopy (HR-TEM) images and selected area electron diffraction (SAED) patterns were taken from a JEOL JEM-2100 Field Emission Transmission Electron Microscope with an accelerating voltage of 200 kV. For the sample preparation of TEM, after ultrasonic agitation of the sample in EtOH, one or more drops of the solution were deposited onto the amorphous carbon film supported on a copper grid (200 mesh) and allowed to dry at 50^{o}C in air. A scanning electron microscope model JSM-7600F (JEOL, Japan) equipped energy dispersive X-ray spectroscopy (EDS) (OXFORD X-Max 80) with was used for morphology and element determination. Powder X-ray diffraction (PXRD) patterns were recorded with X-ray diffractometer equipment model Bruker D8 Advance ECO (Bruker Daltonics) Cu-Kα radiation (λ = 1.5406 Å). Infrared spectrum was measured with a FT-IR spectroscopy model FT/IR 4200 (Jasco, Japan). A surface area analysis equipment model Tri-star 3000 from Micromeretics (Norcross, GA, USA) was employed for surface area measurement of the cMOGs. Raman spectra were performed using Horbia system (iHR320, Horiba Jobin Yvon, France) while the UV-Vis experiments were performed using Shimadzu system (UV-2550, Shimadzu, Japan).

4. Acid-Base Titration

Generally, 5 mg of dried cMOG-N-900 and cMOG-N-500-800 was suspended in 2 mL of 5.88 x 10^{-3} M HCl and 3.68 x 10^{-3} M HCl, respectively, (standardized with NaOH) and magnetically stirred at room temperature for 3 days. After centrifugation (supernatant was set aside), the precipitate was washed with 5 mL D.I. water for three times to remove the unreacted HCl then combined with the supernatant; and subsequently the solution for cMOG-N-500, cMOG-N-600, cMOG-N-700, cMOG-N-800, and cMOG-N-900 was titrated with 4.13 mL, 4.22 mL, 4.23 mL, and 4.34 mL of 3.65 x 10^{-3} M NaOH, and 4.56 mL of 5.12 x 10^{-3} M NaOH solution (standardized with KHP (potassium biphthalate)) to pH 7.0, respectively (Mettler Toledo, Switzerland).

5. Sample Preparation for LDI-MS

The common PCMs used in this study were commercially available. The SWCNT (5–12 nm diameter, > 1 μm length, surface area: ≈ 280 m^2 g^{-1}) (ref. S1) were obtained from Golden Innovation Business Co. Ltd (New Taipei city, Taiwan). Graphite flake (1–10μm, > 99% purity, surface area: ≈ 9 m^2 g^{-1}) (ref. S1) was purchased from Alfa Aesar (Ward Hill, USA). Activated carbon (100–400 mesh, surface area: ≈ 1078 m^2 g^{-1}) (ref. S1) was obtained from Aldrich (Steinheim, Germany). CMK-3 (surface area: ≈ 1000 m^2 g^{-1}; pore diameter: 5.57 nm, total pore volume: 1.35 cm^3 g^{-1}), was purchased from ACS Material. Matrix solution for LDI-MS: A 10 mg of HCCA was dissolved in 1 mL of 0.1% trifluoroacetic acid (TFA). Matrix solution for carbon materials: A 1750 ppm of MOGs or cMOGs was prepared and suspended in 100 μL of EtOH/H_2O (1:1, v/v). For LDI-MS assays, a two-layer approach was used for sample preparation. Briefly, 1 μL of matrix solution was deposited onto the target plate. After drying at room temperature, the analyte solution was then deposited onto the matrix crystals. After 5-10 mins, the plate

with co-crystallized sample was ejected into the instrument for further LDI-MS experiment.

6. Mass Spectrometry

MALDI tandem time of flight mass spectrometry (MALDI-TOF-MS) (Autoflex speed, Bruker Daltonics) equipped with a 355 nm Nd:YAG-laser at 100 Hz was used for analyses. All the analyses were performed under reflectron negative-ion mode. The available accelerating voltage existed in the range from +25 kV to −25 kV. In order to obtain a good S/N ratio, the laser power (25% – 35%) was adjusted to slightly above the threshold.

7. Density Functional Theory (DFT)

The geometry optimization and adsorption energies (E_{ads}) by $DMol^3$ code is based on DFT calculation with spin polarized generalized gradient approximation (GGA) and Perdew-Wang 1991 (PW91) exchange correlation function. All electron calculations were performed for the electron-ion interactions and double numerical basis set including a polarization function (DNP) was selected. The convergence thresholds for the optimization were 2×10^{-5} (energy), 4×10^{-3} (gradient), and 5×10^{-3} (displacement). The E_{ads} is calculated according to the following equation:

$E_{ads} = E[\text{surface + adsorbate}] - (E[\text{surface}] + E[\text{adsorbate}])$, where E[surface + adsorbate], E[surface], and E[adsorbate] are the calculated electron energies of the adsorbed species(aspartic acid) on graphene, and pyridine doped graphene, respectively.

8. Preparation of analyte solutions

The stock solution containing amino acids (aspartic acid (Asp), glutamic acid (Glu), histidine (His), lysine (Lys), arginine (Arg), threonine (Thr), cysteine (Cys), methionine (Met), and phenylalanine (Phe)) was prepared in a 6 mM in deionized water (D.I.) and stored in 4^oC. Before analysis, the solution was diluted to 500 µM using D.I. water. The

nucleobases stock solution (adenine (Ade), cytosine (Cyt)) was prepared in 9 mM in D.I. water then diluted to 0.9 mM before analyses. For peptides (Leu-enkephalin (Leu-Enk), Met-enkephalin (Met-Enk)), the stock solution was prepared in D.I. water (2.5 mM) and then diluted to 100 μM for analyses.

9.

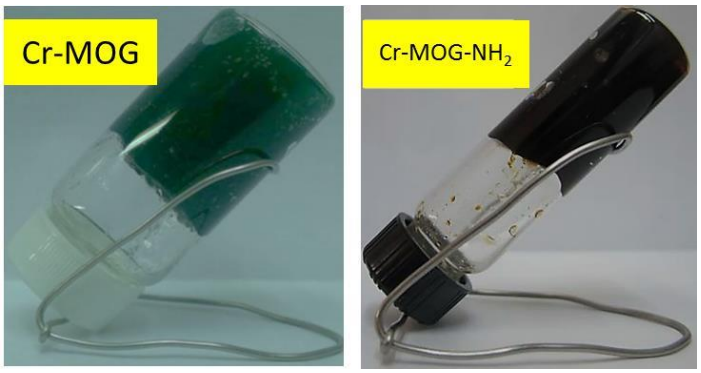

Fig. S1. The optical images of Cr-MOG (left) and Cr-MOG-NH_2 (right).

10.

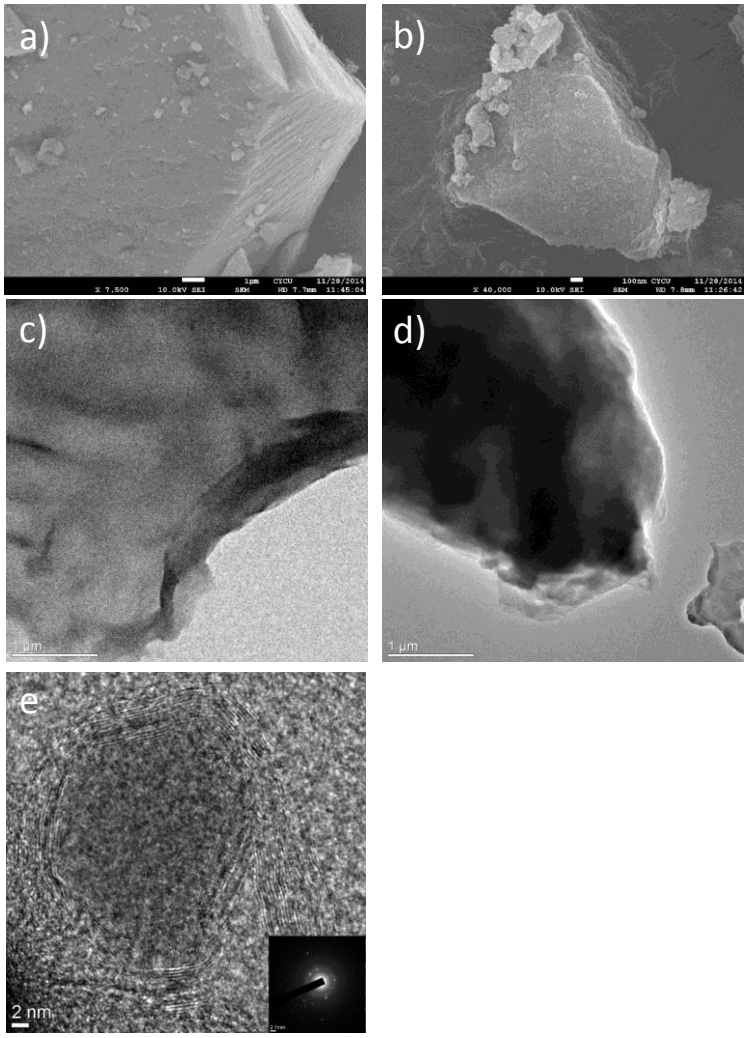

Fig. S2. SEM and TEM images of Cr-MOG (a, c) and Cr-MOG-NH_2 (b, d). HR-TEM images and selected-area electron diffraction (SAED) image (inset) of cMOG-N-900 (e).

11.

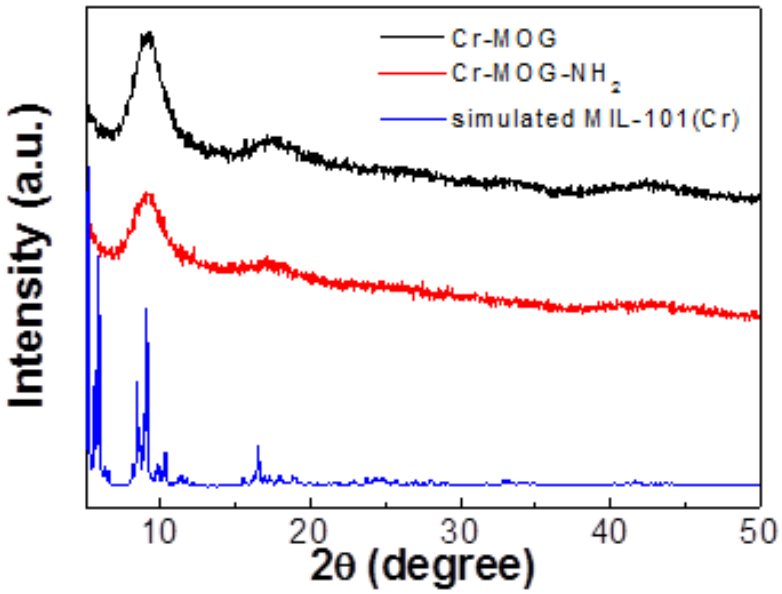

Fig. S3. PXRD pattern spectra of Cr-MOG (black), Cr-MOG-NH_2 (red), and simulated MIL-101(Cr) (black).

12.

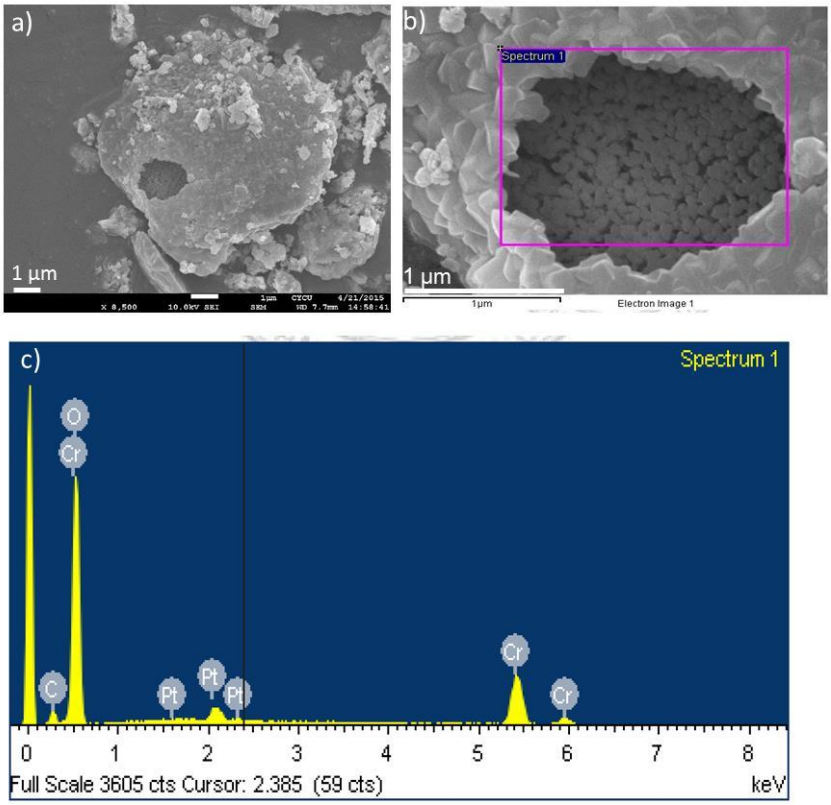

Fig. S4. SEM images of cMOG at magnifications of x 8500 (a) and x 45000 (b). SEM-EDS spectra of cMOG selected in (b).

13.

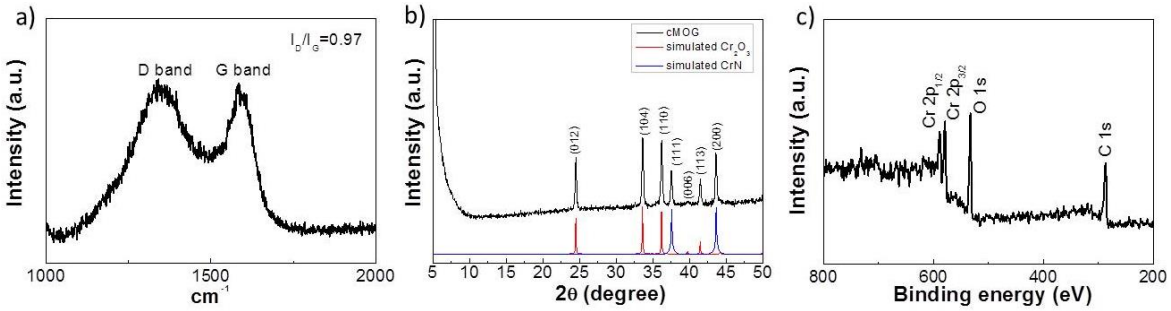

Fig. S5. Characteristic properties of cMOG. a) Raman spectra; b) PXRD pattern; c) Wide range XPS spectra.

14. When the resultant MOG-based PCM and other carbon materials were suspended in aqueous solution for 7 h, well-dispersed black solutions were obtained for cMOG-N and CMK-3 whereas the cMOG and other common carbon materials immediately or gradually precipitated after 1 h, indicating the superiority of cMOG-N in polar and hydrophilic solvents.

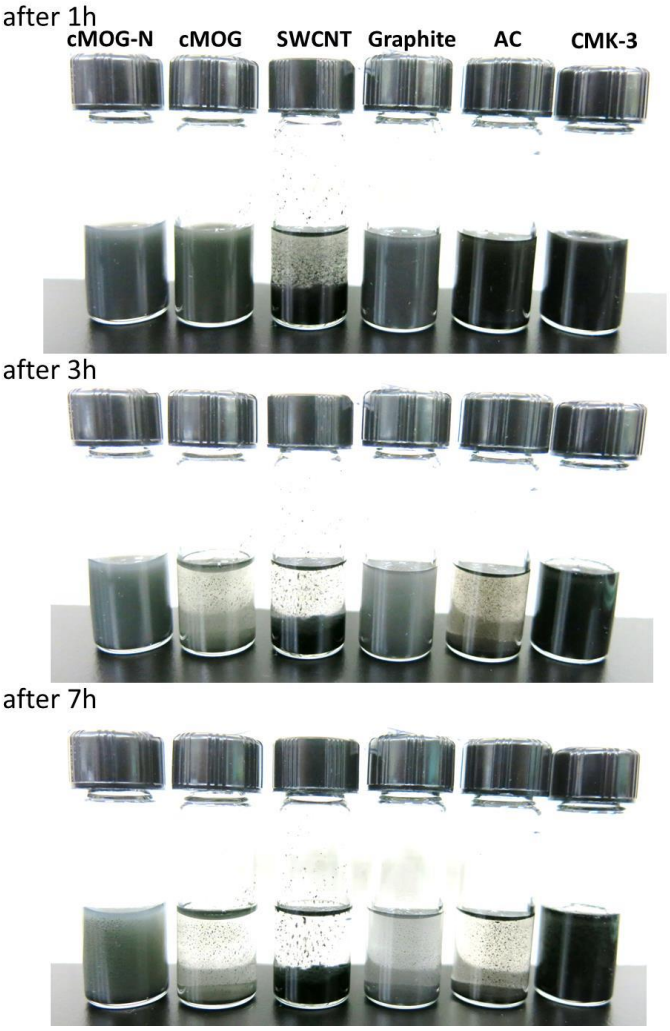

Fig. S6. Dispersibility of carbonized MOGs and other commercial carbon materials in EtOH/H_2O (1:1, v/v) (commonly used solvent for LDI-MS sample preparation). For dispersion, 5 mg of each carbonized MOGs or PCM was suspended in 2 mL solvent.

15.

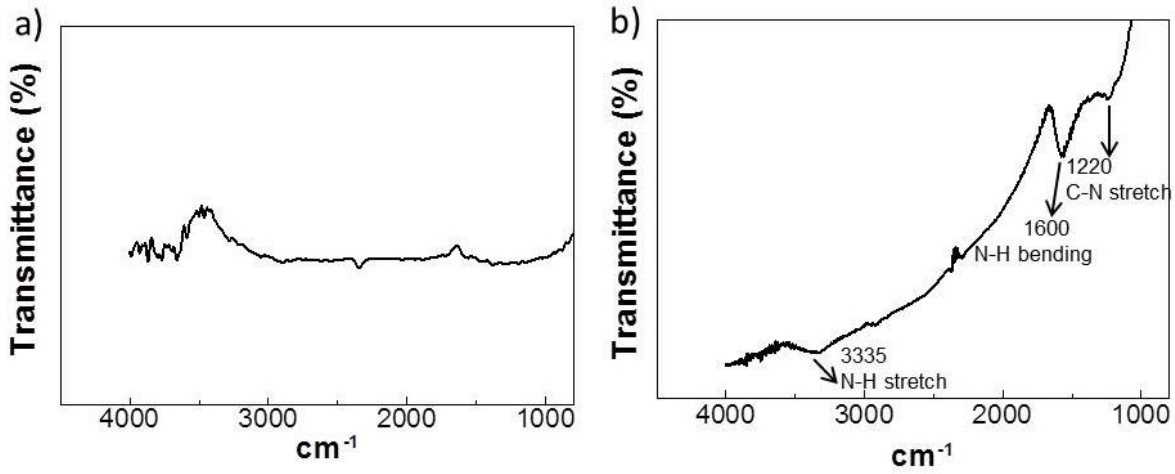

Fig. S7 FTIR spectra of cMOG (a) and cMOG-N (b).

16.

Acid-base titration was also used to determine the nitrogen content for the cMOG-N (500-900). As shown in Fig. S8h, the mol% of nitrogen was also consistent with SEM-EDS results, which decreased from 9.31% to 4.32% as the pyrolysis temperature is increased, demonstrating that the amount of nitrogen in cMOG-N could be adjusted.

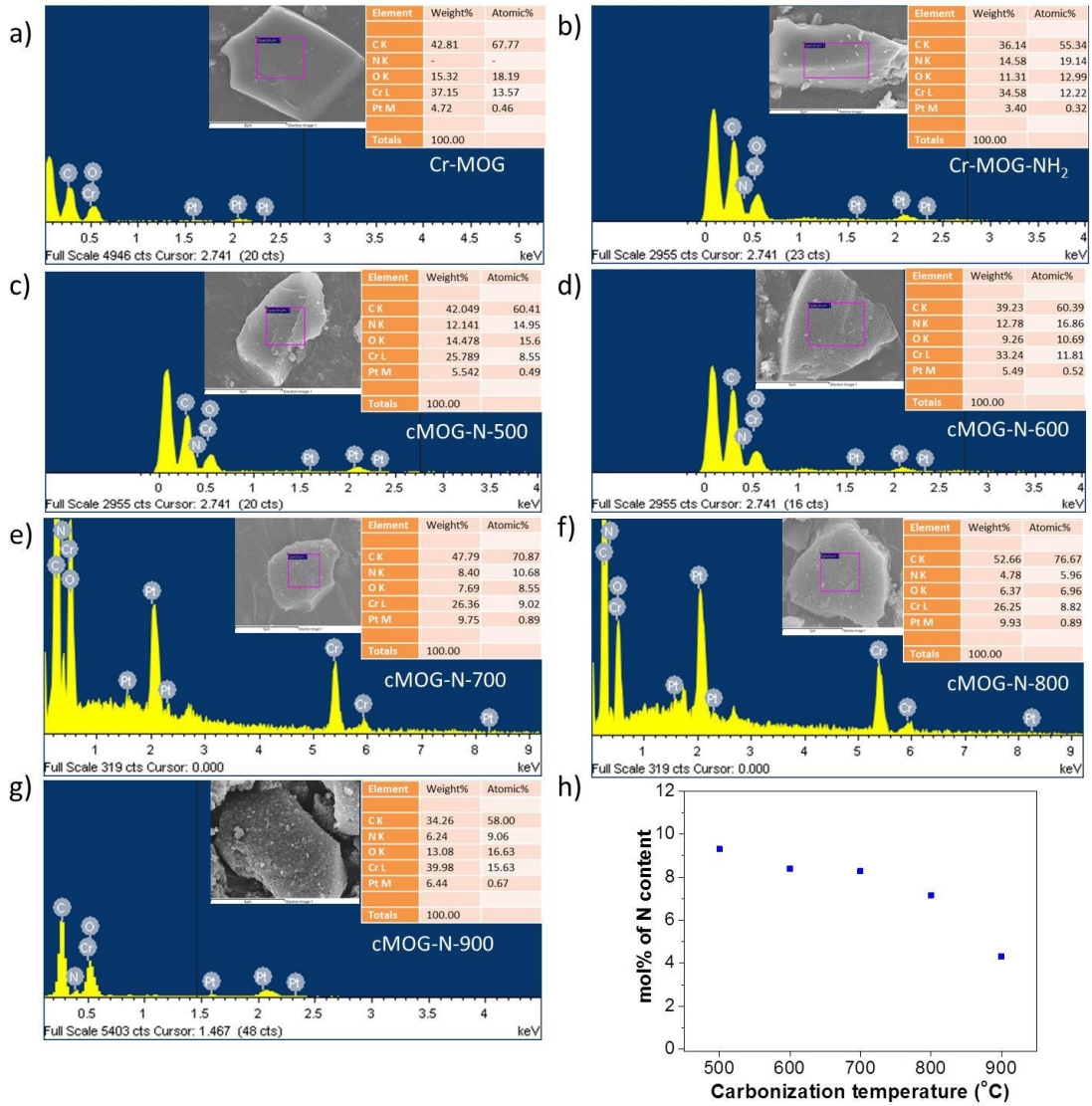

Fig. S8. SEM-EDS analysis of MOGs (a, b) and cMOG-N (500-900) (c-g). The effect of carbonization temperature on nitrogen content in cMOG-N-500-900 (h).

17.

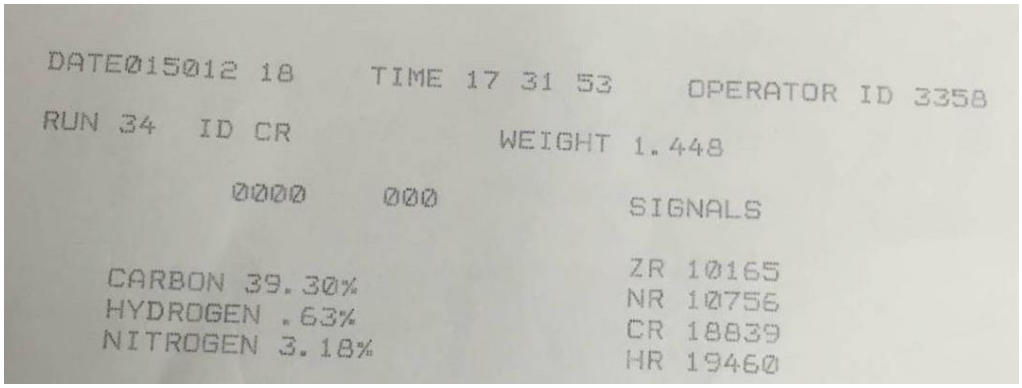

Fig. S9. Element analysis results of cMOG-N.

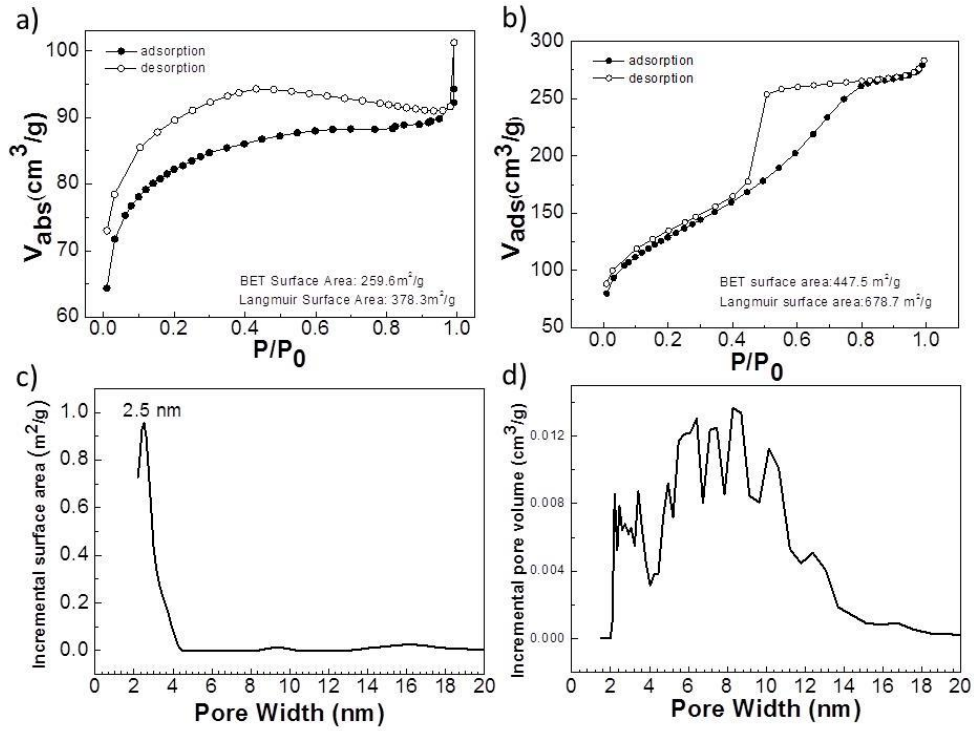

Fig. S10. $N_{2(g)}$ sorption isotherm of a) Cr-MOG and b) cMOG. Pore size distribution of c) Cr-MOG and d) cMOG.

18.

The UV-vis spectra displays higher absorption at 355 nm, a common laser wavelength used in LDI-MS, when Cr-MOG-NH_2 is converted into cMOG-N via direct pyrolysis. Since, the UV-absorbing ability of the matrix highly affects the LDI efficiency of analytes, it is likely that the cMOG-N could generate higher ion yields.

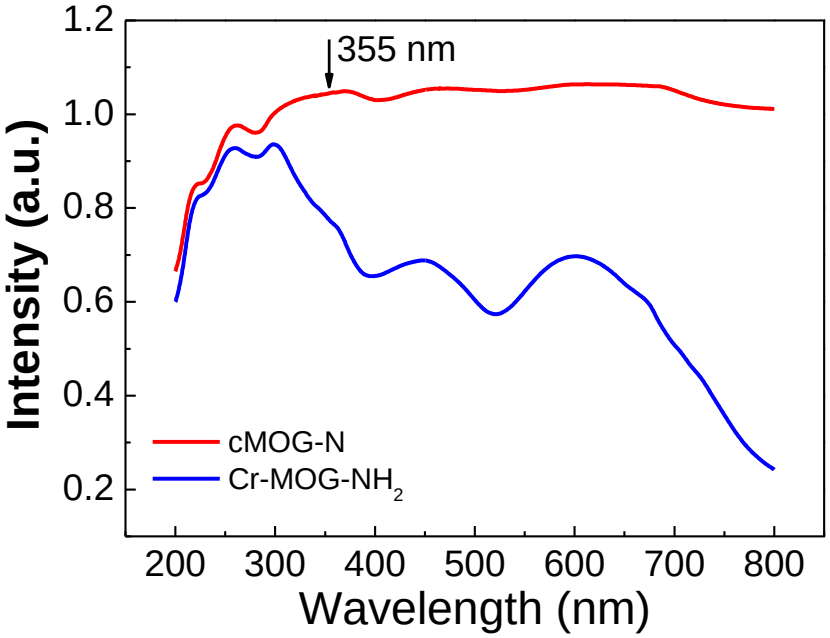

Fig. S11 UV-vis spectra of cMOG-N (red) and Cr-MOG-NH_2 (blue).

19. Direct LDI (without matrix) or MALDI-MS analysis (α-cyano-4-hydroxycinnamic acid (HCCA) as matrix) of amino acids were first investigated. Results show that amino acids signals were not detected without using any matrix (Fig. S12a) while serious background interferences have emerged in low mass region (m/z < 500, Fig. S12b) derived from HCCA matrix, which hinders the detection of analytes.

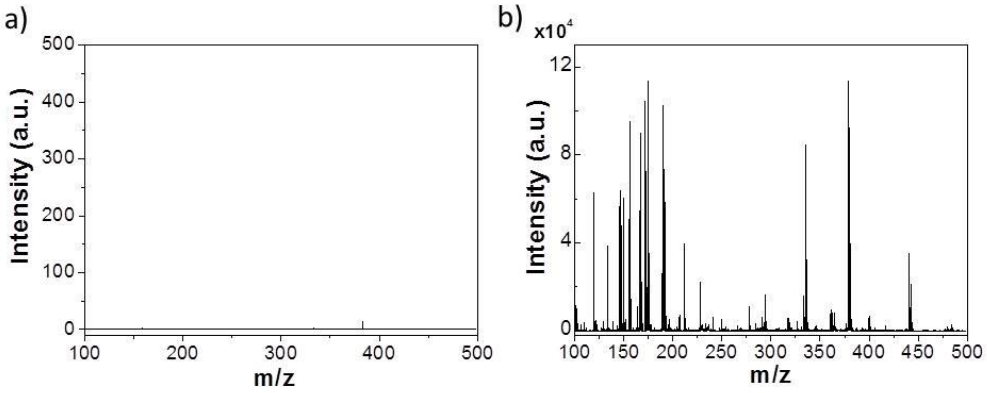

Fig. S12. MS spectra of amino acids analyzed by direct laser desorption/ionization (a) and MALDI with HCCA as matrix (b). Peak identity: Asp ($[M+H]^+$, m/z 134.1); Lys ($[M+H]^+$, m/z 147.2); Glu ($[M+H]^+$, m/z 148.2); His ($[M+H]^+$, m/z 156.2); Arg ($[M+H]^+$, m/z 175.2). Detection mode: positive. Laser: 25%, 500 shots.

20. In order to evaluate the effect of Cr_2O_3 on LDI-MS, we evaluated the effect of Cr_2O_3 on LDI-MS and used a pure Cr_2O_3 as matrix for further analysis. As shown in Fig. S13 (e, f), the absence or very weak amino acid signals can be detected even the laser intensity was increased from 25% to 55%, suggesting that significance of Cr_2O_3 in cMOG-N matrix for LDI-MS is limited. This is probably due to the poor UV-vis absorbability of Cr_2O_3, which is near the range of 355 nm (ref. S2, S3). Furthermore, although the Cr_2O_3 (Lewis acid) was both preserved in cMOG-N and cMOG, the nitrogen characters in cMOG-N, especially for pyridinic-N (Lewis base), provided more significant effect in facilitating the deprotonation of analytes during laser irradiation that resulted in better ionization efficiency than cMOG (i.e negative ion mode) (Fig. S14).

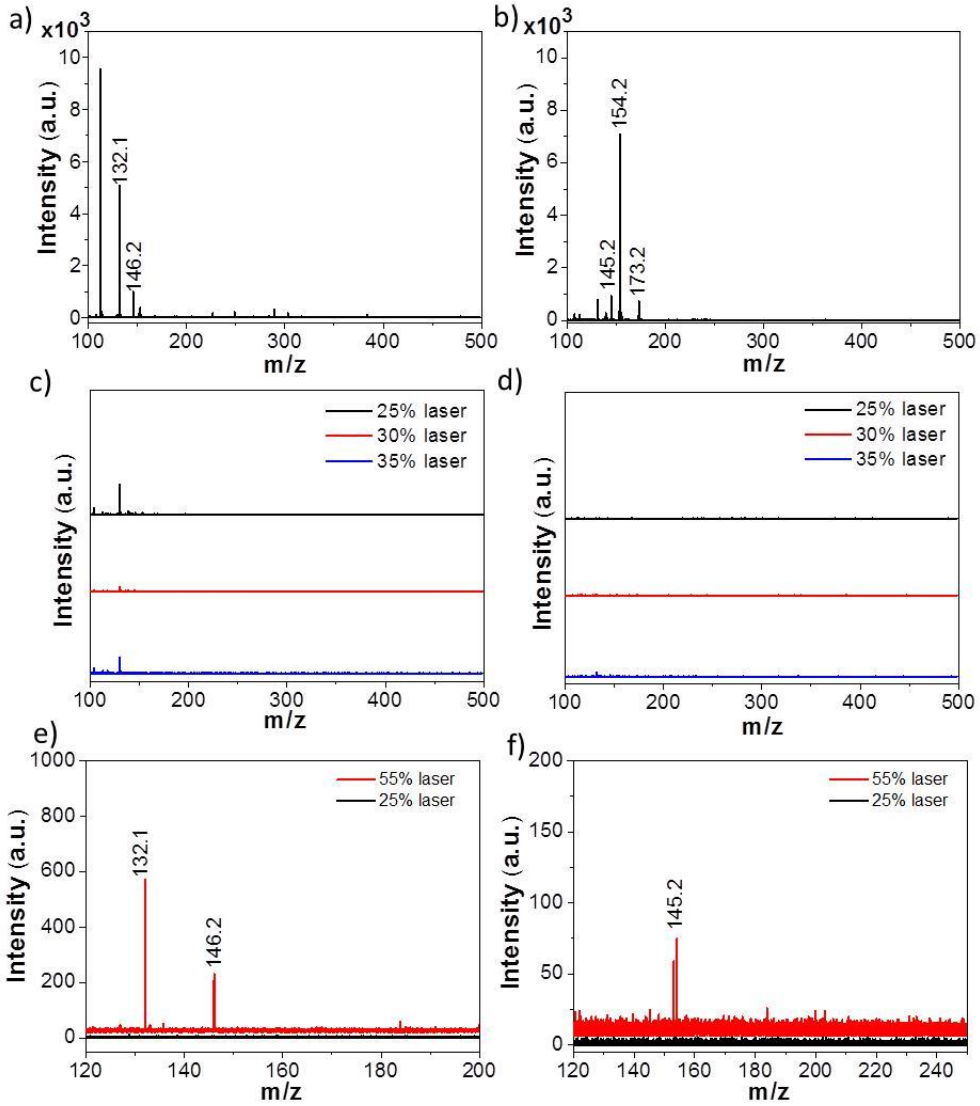

Fig. S13. LDI-MS spectra of (a, c) Asp ($[M-H]^-$, m/z 132.1), Glu ($[M-H]^-$, m/z 146.2), and (b, d) Lys ($[M-H]^-$, m/z 145.2), His ([M-H]-, m/z 154.2), Arg ($[M-H]^-$, m/z 173.2) using cMOG (a, b), Cr-MOG (c, d), and Cr_2O_3 (e, f) as assisted matrix. Detection mode: negative. Laser intensity: 25%, 25-35%, and 25-55% for cMOG, Cr-MOG, and Cr_2O_3, respectively. Laser shots: 500.

21.

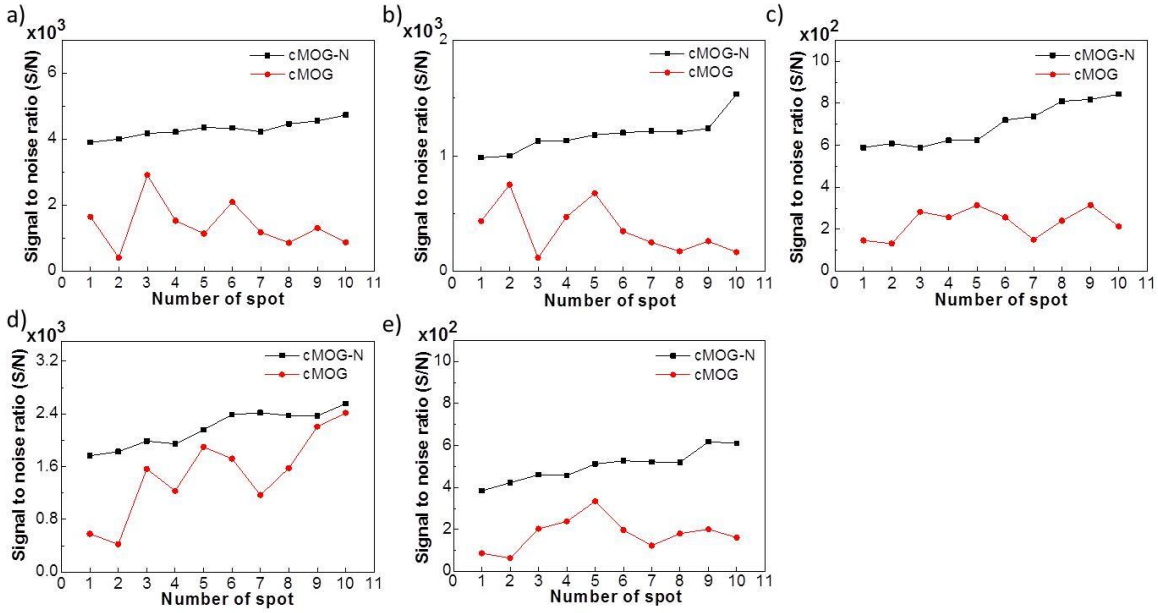

Fig. S14. Signal-to-noise ratio of consecutive ten runs for LDI-MS analysis of a) Asp, b) Glu, c) Lys, d) His, and e) Arg using cMOG-N and cMOG as a matrix.

22.

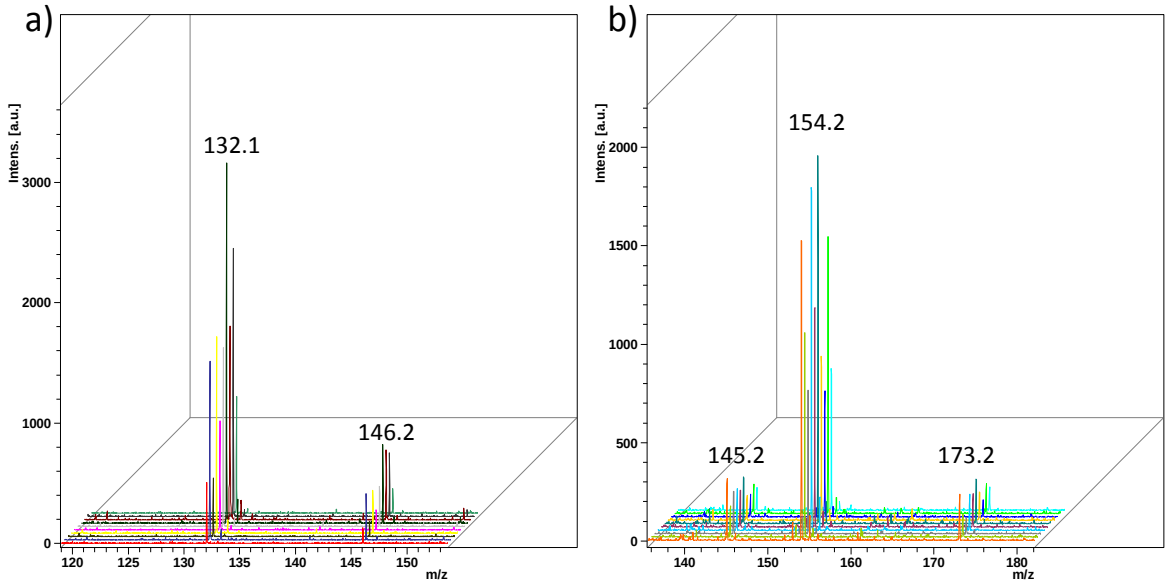

Fig. S15. LDI-MS spectra of (a) Asp ($[M-H]^-$, m/z 132.1) and Glu ($[M-H]^-$, m/z 146.2), and (b) Lys ($[M-H]^-$, m/z 145.2), His ($[M-H]^-$, m/z 154.2) and Arg ($[M-H]^-$, m/z 173.2) using **graphite** as matrix. Detection mode: negative. Laser: 25%, 500 shots.

23.

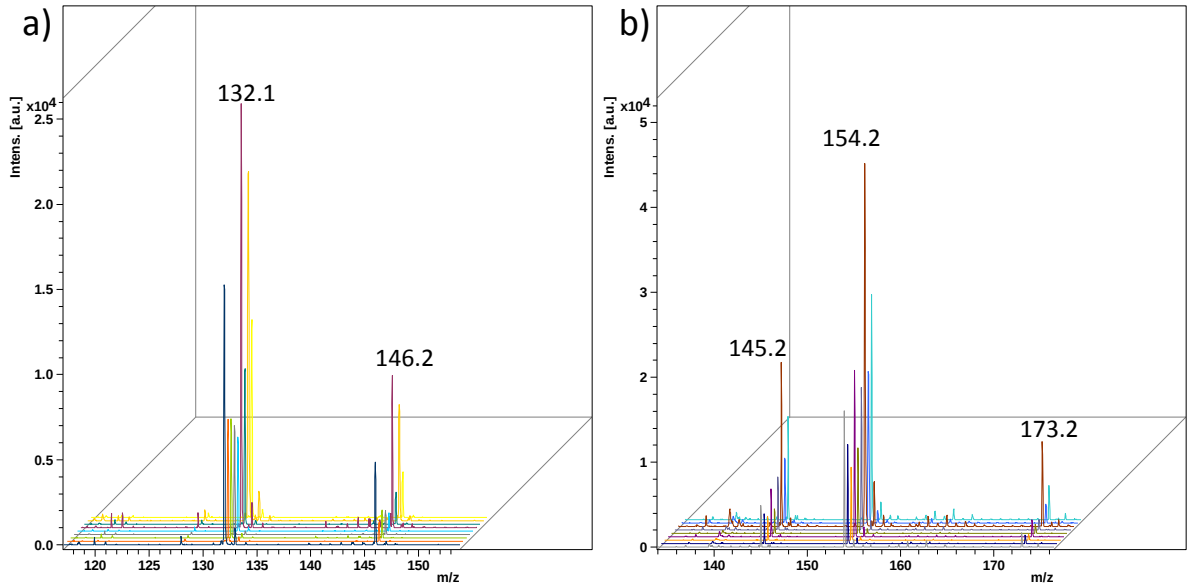

Fig. S16. LDI-MS spectra of (a) Asp ([M-H]$^-$, m/z 132.1) and Glu ([M-H]$^-$, m/z 146.2), and (b) Lys ([M-H]$^-$, m/z 145.2), His ([M-H]$^-$, m/z 154.2) and Arg ([M-H]$^-$, m/z 173.2) using **SWCNT** as matrix. Detection mode: negative. Laser: 25%, 500 shots.

24.

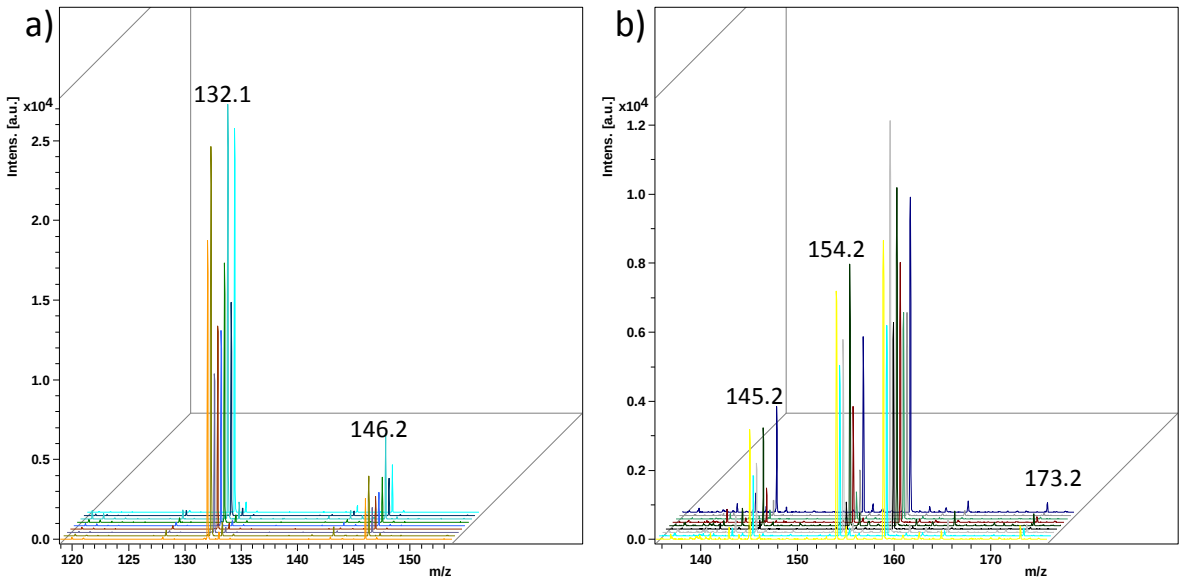

Fig. S17. LDI-MS spectra of (a) Asp ([M-H]$^-$, m/z 132.1) and Glu ([M-H]$^-$, m/z 146.2), and (b) Lys ([M-H]$^-$, m/z 145.2), His ([M-H]$^-$, m/z 154.2) and Arg ([M-H]$^-$, m/z 173.2) using **AC** as matrix. Detection mode: negative. Laser: 25%, 500 shots.

25.

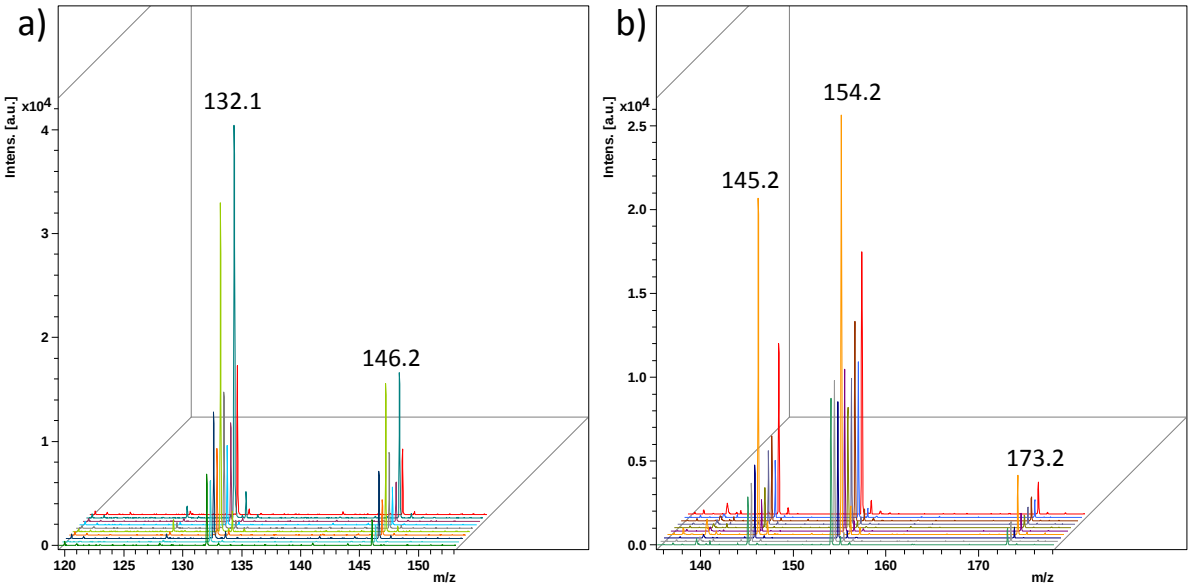

Fig. S18. LDI-MS spectra of (a) Asp ([M-H]$^-$, m/z 132.1) and Glu ([M-H]$^-$, m/z 146.2), and (b) Lys ([M-H]$^-$, m/z 145.2), His ([M-H]$^-$, m/z 154.2) and Arg ([M-H]$^-$, m/z 173.2) using **CMK-3** as matrix. Detection mode: negative. Laser: 25%, 500 shots.

26.

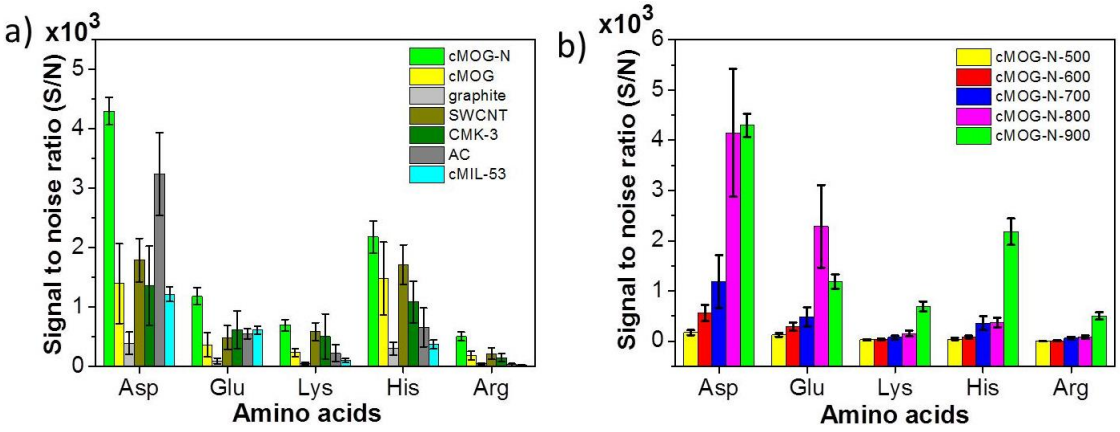

Fig. S19. Comparison of S/N of amino acids using various PCMs as LDI-MS matrix. Data was obtained by ten spectra (n = 10).

27.

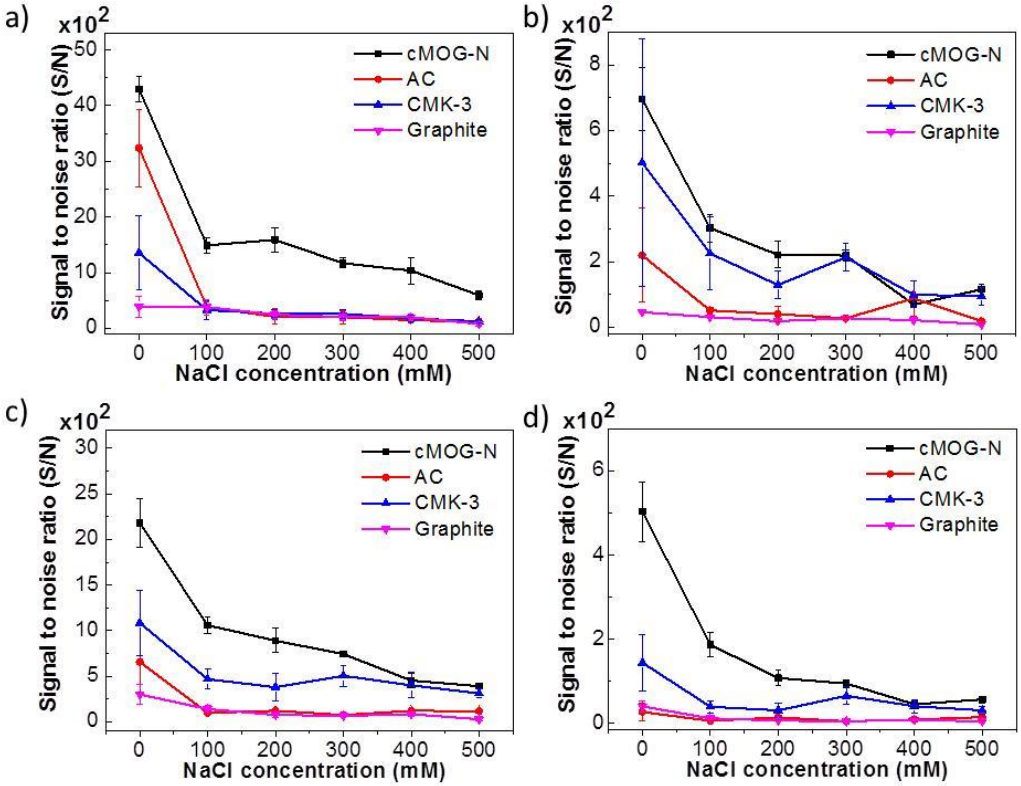

Fig. S20. Salt tolerance of carbonaceous matrices for LDI-MS analysis of amino acids. (a) Asp, (b) Lys, (c) His, and (d) Arg. Each data was averaged by ten mass spectra (n = 10).

28.

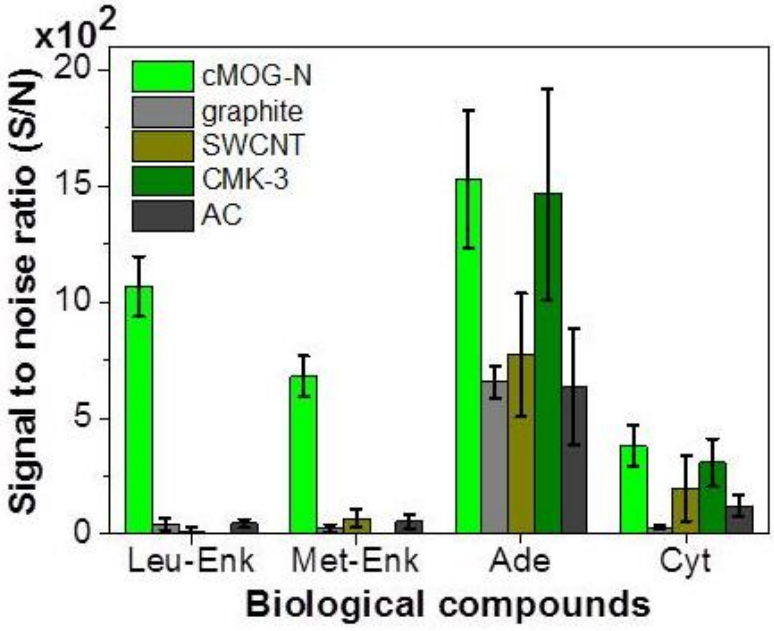

Fig. S21. Comparison of S/N of biological compounds using PCMs as LDI-MS matrix. Data was obtained by ten mass spectra (n = 10).

29.

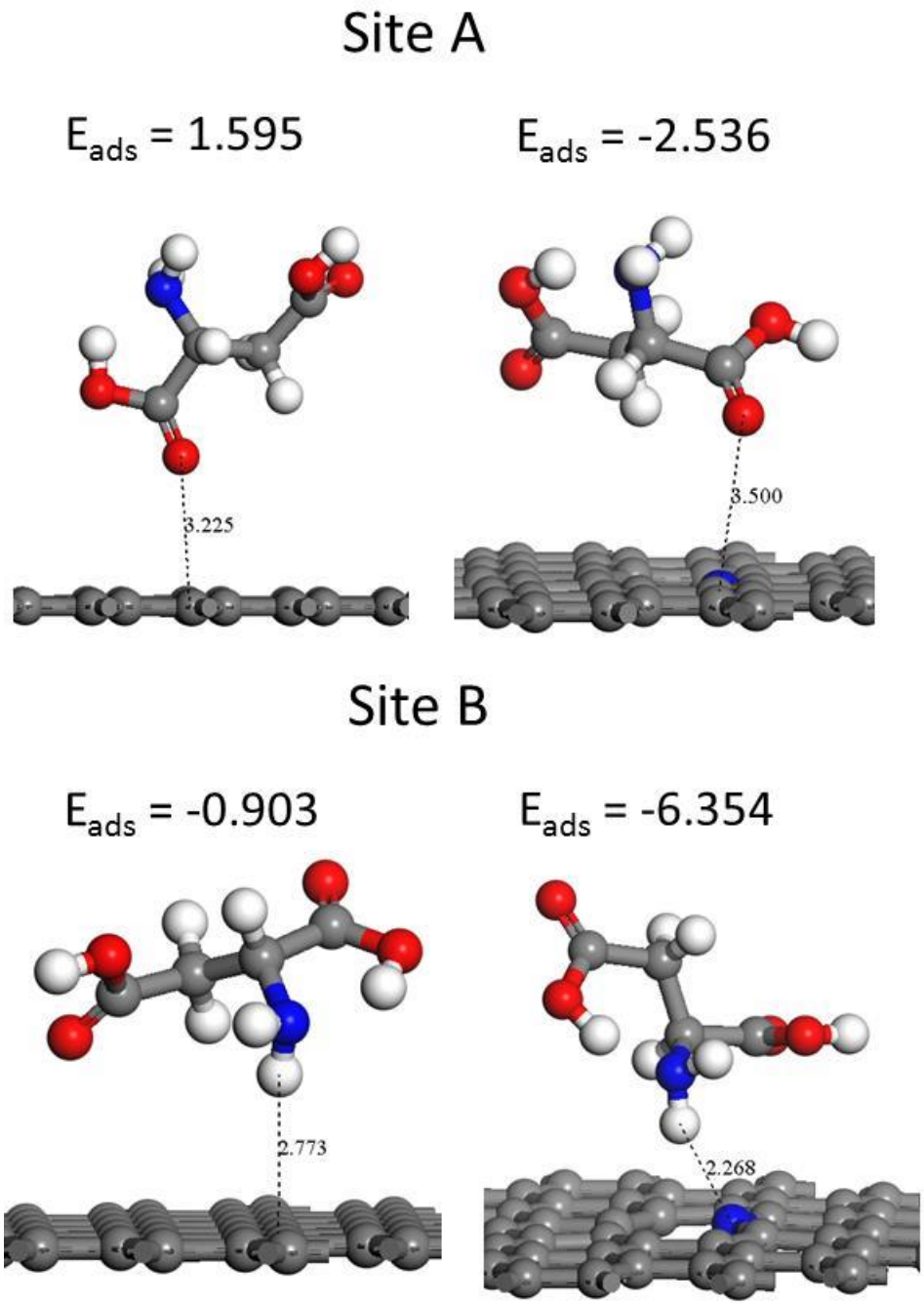

Fig. S22. DFT calculated adsorption sites for aspartic acid in cMOG (left) and cMOG-N (right). Adsorption energies (E_{ads}) are in kJ mol^{-1}, distances in Å. The atoms are shown as follows: H — white, O — red, C — gray, N — blue.

30.

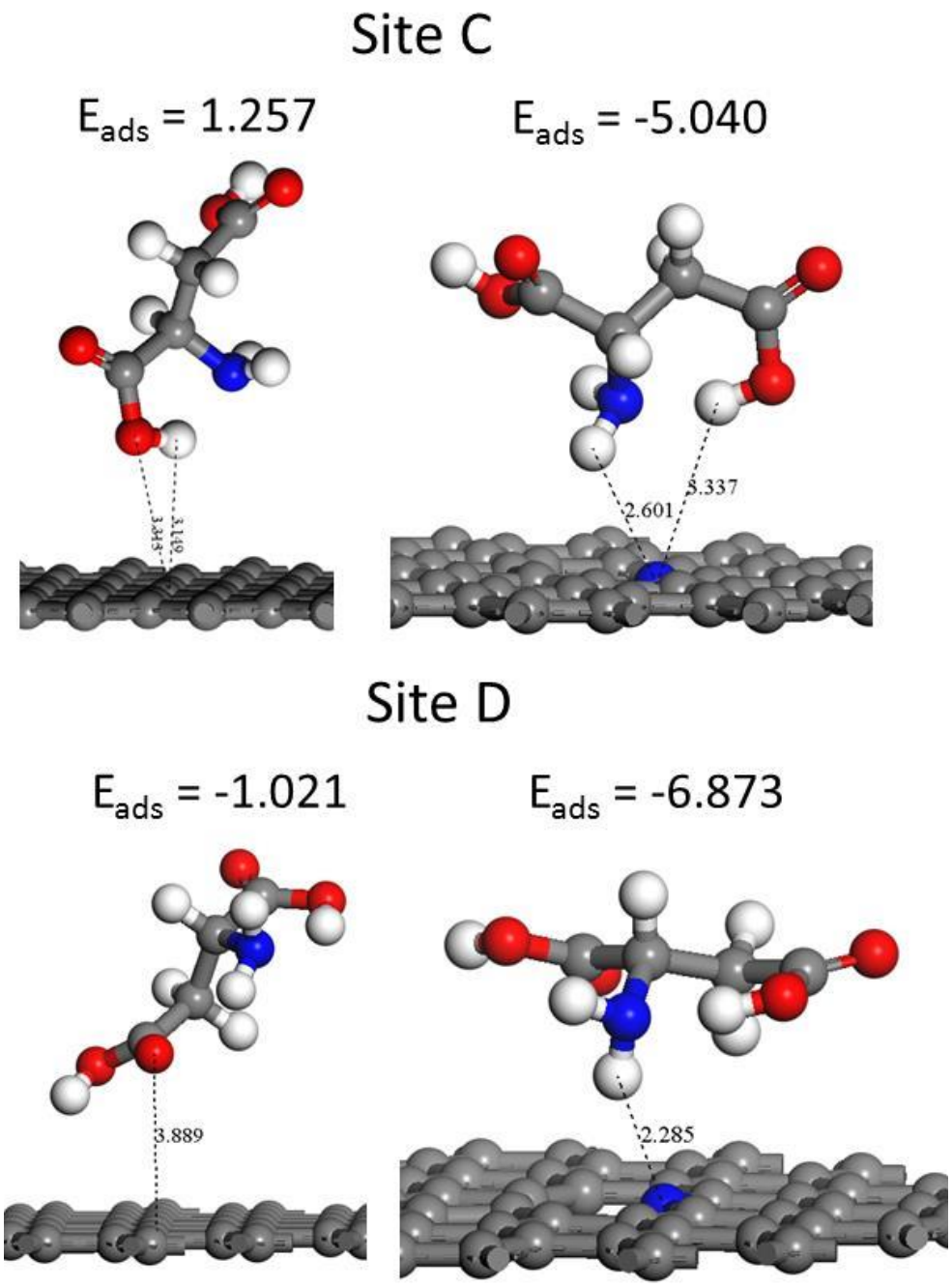

Fig. S23. DFT calculated adsorption sites for aspartic acid in cMOG (left) and cMOG-N (right). Adsorption energies (E_{ads}) are in kJ mol^{-1}, distances in Å. The atoms are shown as follows: H — white, O — red, C — gray, N — blue.

31. Although cMIL-53 matrix has weaker LDI efficiency than cMOG-N, it still preserves better run-to-run reproducibility than other common PCMs (10%-30% of RSD%), indicating that cMIL-53 can reduce the signal variances due to its hydrophilicity but may not promote the negative ionization yields for amino acids. More interestingly, when we changed the detection mode to positive ion mode, the signal intensity is definitely contrary to the negative ion mode and is extremely enhanced by thousand folds (Fig S24c). We suggest that the cMIL-53 functionalized with Lewis acid characters (COOH and Al_2O_3) can act as proton donor to facilitate the production of hydrogen or alkali metal ion adducts.

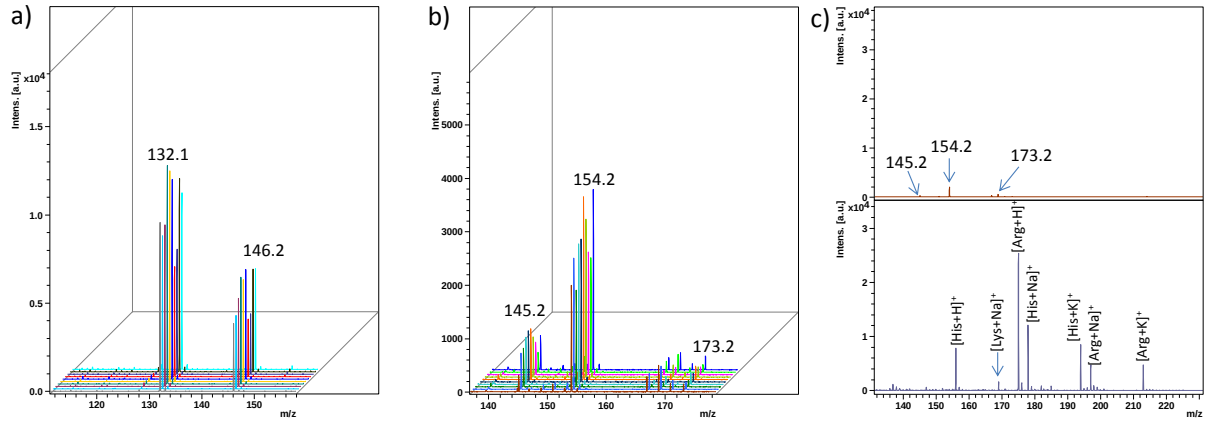

Fig. S24. LDI-MS spectra of (a) Asp ($[M-H]^-$, m/z 132.1) and Glu ($[M-H]^-$, m/z 146.2), (b) Lys ($[M-H]^-$, m/z 145.2), His ($[M-H]^-$, m/z 154.2) and Arg ($[M-H]^-$, m/z 173.2), and (c) His ($[M+H]^+$, m/z 154.1; $[M+Na]^+$, m/z 178.1; $[M+K]^+$, m/z 194.1), Lys ($[M+Na]^+$, m/z 169.1;), and Arg ($[M+H]^+$, m/z 175.1; $[M+Na]^+$, m/z 197.1; $[M+K]^+$, m/z 213.2) using **cMIL-53** as matrix. Detection mode: negative ion mode for (a) and (b), positive ion mode for (c). Laser: 25%, 500 shots.

32.

Table S1. Porosity properties of MOGs and their derivative materials.

	BET surface area (m^2/g)	Pore size distribution (nm)
Cr-MOG	332	2.5
Cr-MOG-NH_2	260	2.5
cMOG	447	2-8
cMOG-N	429	2-12

33.

Table S2. The S/N (RSDs%) of amino acids in LDI-MS assays using different PCMs as matrix[a]

Analytes	cMOG-N-500	cMOG-N-600	cMOG-N-700	cMOG-N-800	cMOG-N-900	cMOG	Graphite	SWCNT	Activated carbon	CMK-3	cMIL-53[b]
Asp	174 (28)	561 (29)	1190 (44)	4149 (31)	4299 (5)	1395 (48)	390 (48)	1790 (20)	3239 (22)	1356 (49)	1215.1 (10)
Glu	128 (31)	289 (28)	484 (39)	2284 (36)	1181 (12)	363 (56)	93 (52)	486 (41)	547 (15)	620 (51)	610.1 (11)
Lys	30 (50)	31 (47)	76 (41)	153 (39)	696 (13)	231 (28)	46 (31)	582 (26)	220 (66)	502 (75)	98.6 (30)
His	45 (47)	80 (36)	362 (38)	379 (25)	2180 (12)	1480 (41)	299 (36)	1712 (20)	657 (50)	1083 (33)	369.7 (20)
Arg	5 (62)	8 (46)	61 (46)	81 (42)	503 (14)	179 (41)	41 (30)	214 (46)	27 (79)	145 (46)	26.5 (25)

[a] Data was calculated from mass spectra by ten consecutive runs.
[b] cMIL-53 was synthesized according to the previous literature.[S1]

34.

Table S3. The S/N ratio (RSDs%) of biological compounds in LDI-MS assay using different PCMs as matrix[a]

Analytes	cMOG-N	Graphite	SWCNT	Activated carbon	CMK-3
Leu-Enk	1067 (12)	44 (57)	390 (48)	47 (38)	-
Met-Enk	679 (13)	25 (63)	93 (52)	56 (55)	-
Ade	1532 (19)	655 (10)	46 (31)	636 (39)	308 (34)
Cyt	381 (22)	29 (22)	299 (36)	120 (39)	1468 (31)

[a] Data was calculated from mass spectra by ten consecutive runs; - unable detection.

Reference

S1. Y.-H. Shih, C.-P. Fu, W.-L. Liu, C.-H. Lin, H.-Y. Huang and S. Ma, *Small*, 2016, **12**, 2057.

S2. M. M. Abdullah, F. M. Rajab, S. M. Al-Abbas, *AIP Advances*, 2014, **4**, 027121.

S3. S. Lei, X. Peng, Z.Liang, X. Li, C. Wang, B. Cheng, Y. Xiao, L. Zhou, *J. Mater. Chem.*, 2012, 22, 1643